

# Designing a practical system for spectral imaging of skylight

Miguel A. López-Álvarez, Javier Hernández-Andrés, Javier Romero, and Raymond L. Lee, Jr.

In earlier work [J. Opt. Soc. Am. A **21**, 13–23 (2004)], we showed that a combination of linear models and optimum Gaussian sensors obtained by an exhaustive search can recover daylight spectra reliably from broadband sensor data. Thus our algorithm and sensors could be used to design an accurate, relatively inexpensive system for spectral imaging of daylight. Here we improve our simulation of the multispectral system by (1) considering the different kinds of noise inherent in electronic devices such as charge-coupled devices (CCDs) or complementary metal-oxide semiconductors (CMOS) and (2) extending our research to a different kind of natural illumination, skylight. Because exhaustive searches are expensive computationally, here we switch to a simulated annealing algorithm to define the optimum sensors for recovering skylight spectra. The annealing algorithm requires us to minimize a single cost function, and so we develop one that calculates both the spectral and colorimetric similarity of any pair of skylight spectra. We show that the simulated annealing algorithm yields results similar to the exhaustive search but with much less computational effort. Our technique lets us study the properties of optimum sensors in the presence of noise, one side effect of which is that adding more sensors may not improve the spectral recovery. © 2005 Optical Society of America

OCIS codes: 010.1290, 150.0150, 150.2950, 040.0040.

## 1. Introduction

No one nowadays would attempt to analyze naked-eye atmospheric phenomena such as rainbows, halos, glories, or coronas without using instruments. Daylight and skylight spectra, for example, are normally measured with spectroradiometers, which are complex and expensive instruments that provide only one spectrum per measurement. Thus when one measures skylight, the illumination arrives from either a small or large angular subtense of the sky, depending on the instrument field of view. Because researchers could benefit from high-resolution angular maps of skylight's spectral power distribution (SPD), we need to measure many skylight spectra simultaneously across the sky dome. Multispectral imaging systems let us do so.

In recent years the development and design of mul-

tispectral color-image acquisition devices has received much attention in color science. By extending our past research on sky color,<sup>1–4</sup> we offer here a theoretical optimum design of a multispectral system with 3–5 channels that can recover the SPD of the skylight incident on it. Our optimum multispectral system must estimate the spectral skylight radiance at each pixel of the image based on the response of the system's channels. This is a classic inverse problem that requires a mathematical estimation algorithm. We opt for a linear model based on a principal components analysis (PCA) described in Section 2.

In the future, we plan to build a multispectral system for imaging skylight by using liquid-crystal tunable filters (LCTFs) and a linear monochrome camera with high dynamic range. Therefore our simulated system must model the behavior of the optimum sensors realistically, including the effects of sensor noise (see Section 3).

Any search for an optimum set of Gaussian sensors (those whose spectral sensitivities are Gaussian functions of wavelength) intended to recover skylight spectra with a multispectral imaging system depends on several factors: the spectral response of its sensors, the type and number of sensors, and the noise that always affects any electronic device. To include all these factors in an exhaustive search is a highly demanding computational task. Our alternative ap-

---

M. A. López-Álvarez, J. Hernández-Andrés (javierha@ugr.es), and J. Romero are with Departamento de Óptica, Facultad de Ciencias, Universidad de Granada, 18071 Granada, Spain. R. L. Lee is with the Mathematics and Science Division, United States Naval Academy, Annapolis, Maryland 21402.

Received 21 December 2004; revised manuscript received 27 April 2005; accepted 3 May 2005.

0003-6935/05/275688-08\$15.00/0

© 2005 Optical Society of America

proach greatly reduces computing time with a simulated annealing algorithm that minimizes a cost function (see Section 4). To this end, we propose a single cost function that evaluates the quality of our recovered skylight spectra: the colorimetric and spectral combined metric or CSCM function.

In Section 5 we present the results of both recoveries for two different sets of skylight spectra. One dataset was measured in Granada, Spain, and was used as a training set both in the PCA and in the simulated annealing algorithm. The second dataset was measured in Owings, Maryland, and was used to test the accuracy of our simulated spectral imaging system.

## 2. Estimating Skylight Spectra from Broadband Sensor Data

The spectral response of CCD camera sensors is often assumed to be linear.<sup>5–7</sup> If we make this assumption for our multispectral imaging system, we can model its sensors' response using

$$\rho_k = \int_{\lambda_{\min}}^{\lambda_{\max}} E(\lambda)R_k(\lambda)d\lambda, \quad (1)$$

where  $\rho_k$  is the response of  $k$ th sensor,  $E(\lambda)$  is the illuminant spectrum (skylight in our case), and  $R_k(\lambda)$  is the  $k$ th sensor's spectral sensitivity. If we sample the visible spectrum at  $N$  different wavelengths, Eq. (1) is

$$\rho_k = \sum_{m=1}^N E(\lambda_m)R_k(\lambda_m). \quad (2)$$

In an earlier paper,<sup>2</sup> we measured 1567 skylight spectra in Granada, Spain (37° 10'N, 3° 36' W, elevation 680 m) at many different solar elevations; each spectrum ranged from 380 – 780 nm in 5 nm steps. This dataset allowed us to obtain 81 eigenvectors from a principal components analysis<sup>8,9</sup> (PCA). The eigenvectors  $V_n(\lambda_m)$  can then be used in a linear model to reconstruct a given skylight spectrum by

$$E(\lambda_m) = \sum_{n=1}^N \varepsilon_n V_n(\lambda_m). \quad (3)$$

This PCA-based linear reconstruction method has been used widely<sup>5,6,8–16</sup> and gives good results compared with other estimation methods (such as Wiener's method, spline interpolation, modified discrete sine transform, nonnegative matrix factorization, or direct transformations).<sup>12,16,17</sup>

The weight  $\varepsilon_n$  of each principal component in the linear combination is calculated from a camera's sensitivity (or sensor response) spectra. If we substitute Eq. (3) in Eq. (2) and express it in matrix form, then

$$\rho = R^T V \varepsilon = \Lambda \varepsilon, \quad (4)$$

where  $\rho$  is a vector of  $k$  rows containing the  $k$  sensors' responses,  $R$  is an  $N \times k$  matrix containing the spectral sensitivities of the  $k$  sensors at  $N$  sampled wavelengths (superscript  $T$  denotes its transpose),  $V$  is a  $N \times n$  matrix containing the first  $n$  eigenvectors used in reconstructing  $N$  wavelengths, and  $\varepsilon$  is a vector of  $n$  rows that contains the coefficients of Eq. (3)'s linear combination. Then  $\Lambda$  is a  $k \times n$  matrix that directly transforms the coefficients  $\varepsilon$  into the sensor responses  $\rho$ . By calculating  $\Lambda$ 's pseudoinverse (denoted by superscript  $+$ ), we obtain the coefficients for the linear estimate of the camera sensor responses, and then we can recover the skylight spectrum

$$E_R(\lambda_m) = V \Lambda^+ \rho. \quad (5)$$

So with a combination of  $k$  sensors and  $n$  eigenvectors, we can estimate skylight spectra using Eq. (5). Note that  $k$  and  $n$  need not be equal, although we find that this often gives the best results.

## 3. Influence of Noise

Any real imaging system is of course affected by noise,<sup>5</sup> a fact not explicitly accounted for in Eqs. (1)–(5). Yet noise can be represented there as an additive term that changes the ideal noise-free sensor responses to

$$\rho_{\text{noise}} = \rho + \sigma, \quad (6)$$

where  $\sigma$  is a  $k$ -row vector of uncorrelated components that affect each sensor separately. There are various sources of noise,<sup>18</sup> with *thermal noise* being the most common. This consists of random, normally distributed white noise (i.e., affecting every wavelength equally) that is additive and whose variance increases with temperature. Another noise source in electronic systems is *shot noise*, whose source is current fluctuations in semiconductor devices due to the quantum character of electrons. Although shot noise is insignificant compared with thermal noise in metal-oxide semiconductor (MOS) devices such as CCDs, it too is normally distributed. *Flicker noise* is also common, and it varies inversely with camera electric frequency (the temporal frequency at which pixels charges are read). Finally, *quantization noise* is present in every analog-to-digital (A/D) conversion and is the loss of least-significant digits when quantizing scene radiances to a given number of bits (i.e., to a fixed number of discrete levels).

In this study, we simulate thermal and shot noise as random, normally distributed noise with standard deviations of 1%, 3%, or 5% of the maximum sensor response (these noise levels correspond to signal-to-noise ratios (SNRs) of 40 dB, 30 dB, and 26 dB, respectively). Quantization noise is given as that due to A/D conversion at resolutions of 8, 10, or 12 bits. This slightly degraded performance closely approximates the behavior of a real multispectral imaging system.

Table 1. Means and Standard Deviations (SD) for 1567 Skylight Spectra Measured in Granada, Spain, Using 3 Sensors, 3 Eigenvectors, and 12-Bit Quantization in Recovering Spectra at Different Signal-to-Noise Ratios (SNR)

SNR	GFC $\pm$ SD	$\Delta E^*_{ab}$ $\pm$ SD	IIE(%) $\pm$ SD	LN(1 + 1000(1 - GFC)) $\pm$ SD	CSCM $\pm$ SD
40 dB	0.9993 $\pm$ 0.0012	0.7 $\pm$ 0.5	1.3 $\pm$ 0.7	0.4 $\pm$ 0.3	2.4 $\pm$ 1.1
30 dB	0.9987 $\pm$ 0.0016	0.9 $\pm$ 0.5	3.2 $\pm$ 1.9	0.7 $\pm$ 0.4	4.8 $\pm$ 2.2
26 dB	0.9981 $\pm$ 0.0023	1.3 $\pm$ 0.7	5.0 $\pm$ 3.5	0.9 $\pm$ 0.5	7.3 $\pm$ 4.1

#### 4. Searching for Optimum Sensors

Various methods have been proposed for selecting the optimum filters or sensors for a multispectral imaging system.<sup>5-7,14,17,19</sup> However, no consensus exists about what “optimum” means in such a system. For us, one set of sensors is clearly better than another if its reconstructed skylight spectra are more accurate when tested by some metric. The key question is what metric to use.

For our problem, essentially two kinds of metrics exist: colorimetric and spectral.<sup>20</sup> Colorimetric metrics formulated by the CIE (Commission Internationale de l’Éclairage), include CIELUV, CIELAB, CIE94, and CIEDE2000.<sup>21,22</sup> These metrics quantify distances in their respective quasi-uniform color spaces and approximate color differences observed by the human eye. To calculate such metrics, we only need to know the tristimulus values<sup>23</sup> of a given color signal. Note that any skylight color can be quantified by spectrally convolving its SPD with each of three CIE color-matching functions (we use functions for the 2° 1931 CIE standard observer). Integrals of the three convolved spectra yield the particular skylight color’s tristimulus values. This trichromatic matching has a major consequence: we cannot distinguish between metamers, which are color stimuli with the same tristimulus values but different SPDs. Spectral metrics are those that measure the distance between two spectral curves, such as root-mean-square error (RMSE) or goodness-fit coefficient<sup>2</sup> (GFC, which uses Schwartz’s inequality, a widely accepted<sup>20,24</sup> index of similarity between two spectra). These metrics distinguish between metamers but do not consider human vision. Some new metrics have been proposed for comparing spectra that take into account properties of the human visual system, such as weighted RMSE (WRMSE) with the diagonal of Cohen matrix  $R$ .<sup>20</sup> Viggiano proposed a spectral comparison index<sup>25</sup> (SCI), a metric whose properties have been studied by others.<sup>20,24,25</sup> Another metric widely used in solar radiation measurements is the percentage of the integrated irradiance error<sup>26</sup> (IIE(%)) across the visible spectrum.

Some authors<sup>6</sup> have searched for optimum sensors using only one of the metrics described above. Because their results depend on the metric used, they are not particularly useful in selecting sensors for our planned multispectral system. Imai *et al.* suggest that “mononumerosis” should be avoided when evaluating the quality of spectral matches.<sup>20</sup> By this term they mean that *several* metrics should be used to

assess color reconstruction from both colorimetric and spectral standpoints. Day<sup>14</sup> used thresholds for RMSE and CIEDE2000 metrics when searching for optimum sensors; Hernández-Andrés *et al.*<sup>1</sup> used GFC, CIELUV, and IIE(%) in a similar way.

As explained below, we must use a single cost function when developing a simulated annealing algorithm. This approach may seem to contradict the recommendations of Imai *et al.*<sup>20</sup> Yet it does not, because we actually construct a simple single-cost function or metric that combines several metrics at once. We use GFC as a spectral metric, CIELAB as a colorimetric cost function (denoted by  $\Delta E^*_{ab}$ , the distance between two colors in the CIE’s uniform color space  $L^*a^*b^*$ ), and IIE(%) as a metric for comparing the spectral curves of natural illuminants. In principle, our new metric should approach zero for near-perfect matches (in contrast with GFC, which tends to unity for perfect matches) and give approximately the same weight to the GFC, CIELAB, and IIE(%) metrics. As defined in Section 1, our combined CSCM metric is calculated by

$$\text{CSCM} = \text{Ln}(1 + 1000(1 - \text{GFC})) + \Delta E^*_{ab} + \text{IIE}(\%). \quad (7)$$

Equation (7) defines a combined metric that is zero for perfect matches, and thus is a good candidate for developing an annealing search algorithm. The chief advantage of this metric is that it quantifies the following: spectral mismatches among metamers, perceptual differences in color matches, and differences in such integrated radiometric quantities as irradiance or radiance. Though this metric may not avoid “mononumerosis,” it clearly combines the properties of various metrics relevant to skylight spectra.

Table 1 shows the means and standard deviations (SDs) for our Granada skylight spectra obtained using the linear method described above for the 3 best sensors (as described later) and 3 eigenvectors at various noise levels (always with 12-bit quantization). Note that the GFC, CIELAB, and IIE(%) terms are roughly equal in each row of Table 1, thus justifying our weights for them in Eq. (7).

Now that Eq. (7) quantitatively defines our optimum sensor, we next turn to developing a search algorithm. Whenever possible, one should do an exhaustive search to find a multispectral system’s optimum sensors. Yet such a search can demand excessive computer time because the number of possible filter sets can be enormous. We perform our

study using 3–5 sensors that are Gaussian functions of wavelength.<sup>6,7,10,17</sup> These sensors are similar to commercial ones and could also be made using a LCTF. We vary sensors' peak sensitivities from 380 – 780 nm in 5 nm steps, a spectral resolution adequate for both colorimetry and radiometry. We also vary the sensors' FWHM (full width at half maximum) from 10 – 300 nm in 10 nm steps. Finally, we perform linear spectral recoveries using 3, 4, and 5 eigenvectors. To appreciate the computational burden involved, note that  $\sim 10^{10}$  different sets must each be evaluated to find the optimum set for a 3–sensor system, a search that requires several days on existing personal computers. This huge number grows if we try to find the best 4 or 5 sensors, for which the task is now unfeasible because the numbers of possible sets increase by factors of  $10^3$  and  $10^6$ , respectively.

Faced with such daunting computational challenges, we turn to *simulated annealing* algorithms that greatly speed the finding of optimum solutions to a system with many different sets of sensors. If we slightly relax our requirements for recovery accuracy, an annealing algorithm can give a nearly optimum solution after testing only  $\sim 10^5$  sets of sensors. Indeed, an annealing algorithm gives ever-better solutions the longer we let it run, in contrast with an exhaustive search in which simulation time is not a variable that can be chosen *a priori*.

Simulated annealing algorithms have been widely used as search algorithms in physics<sup>27,28</sup> and in the design of multispectral imaging systems,<sup>6,17</sup> but typically they evaluate only a single metric such as CIELAB  $\Delta E^*_{ab}$  or spectral RMSE. Such algorithms are based on simulating the process of annealing (slow cooling after heating) of a thermodynamic system (e.g., a gas) that is always in thermal equilibrium. The algorithm searches for the minimum energy state when temperature decreases with time, or at least for a local minimum from which the system will not move without an enormous energy perturbation, a condition not found in thermal equilibrium. We must construct a rule for changing the existing state, calculate its energy, and accept it as the system state with a probability given by Boltzmann's factor  $e^{-\Delta E/KT}$ . In our case, energy is replaced with Eq. (7)'s CSCM cost function, and this substitution makes clear why the CSCM must be a single function that equals zero for perfect matches. The state is represented by a given set of sensors (the peak sensitivities and FWHM of which determine the energy of the state), and the rule of state-changing will statistically favor those states whose energy is close to that of the current state.

We have compared the efficiency of the simulated annealing algorithm with an exhaustive, yet feasible, search across 3 sensors. We performed the exhaustive search together with the simulated annealing search using (1) the CSCM as a single cost function and (2) various random additive noise levels, always with 12 bits for quantization noise (Table 2). In most cases

the annealing algorithm found the same optimum solution as the exhaustive search. In all other cases, the two algorithms' solutions were quite similar, and the shapes of the sensors sensitivity curves were nearly identical. This suggests that the local minimum given by the annealing algorithm is usually equivalent to that obtained by the exhaustive search.

## 5. Results

In this section we present the best sensors obtained with the simulated annealing algorithm in various cases. We first examine the influence of the cost function by restricting ourselves to just 3 sensors. Then we use CSCM exclusively to study the influences of noise, number of sensors, and number of eigenvectors on sensor spectral sensitivities. Our larger goal is to determine general properties of the sensors for our planned multispectral imaging system.

As noted above, some authors use only one metric in their simulated annealing algorithms to find the best sensors for a multispectral system.<sup>6,17</sup> Connah *et al.* found that using RMSE as a cost function produced sensors evenly distributed across the visible spectrum.<sup>6</sup> When they used CIELAB, they obtained sensors with sensitivity spectra similar to those of human cones.

As Table 3 shows, using only a single metric produces sensors that work well according to that metric but that perform poorly according to the other metrics. In particular, CIELAB alone should not be used as a cost function because its small  $\Delta E^*_{ab}$  errors come at the price of large GFC and IIE(%) errors. Thus we use the CSCM, which strikes a balance between the three different metrics.

In a second round of simulations, we looked for the best set of 3, 4, and 5 sensors to recover our Granada skylight spectra using the linear model with 3, 4, and 5 eigenvectors at various noise and quantization levels.

Figure 1 shows that for a given number of sensors, the peak sensitivities and FWHM are similar at different noise levels for the 3–5 eigenvectors used in each linear reconstruction of a skylight spectrum. This behavior is desirable in a practical multispectral system. As other authors have noted,<sup>7,10</sup> sensor sensitivity curves tend to sharpen when the noise is high (i.e., low SNR). This occurs because sharper sensors make the matrix  $\Lambda$  more robust to noise by decreasing its condition number. Not surprisingly, the curves also sharpen as we increase their number (i.e., as we approach a narrow-band hyperspectral imaging system).

Table 4 compares the mean values of the metrics used in this study for our Granada skylight spectra recovered with the best sets of sensors. Both Table 4 and its graphical representation in Fig. 2 show that for low noise (i.e., high SNR), recovered skylight spectra are more accurate if we (1) increase the number of sensors and (2) match the number of eigenvectors and sensors.<sup>15</sup> The former effect occurs because we can sample the visible spectrum more reliably with 5 sensors than with 3, although differences in the metrics are not large.

**Table 2. Comparison of Exhaustive and Simulated Annealing Searches for the Granada Skylight Spectra Recovered with 3 Sensors at 12-Bit Quantization for Different SNR<sup>a</sup>**

SNR	Search	Number of Eigenvectors	Peak Sensitivities (nm)			FWHM (nm)			CSCM $\pm$ SD
			1st Sensor	2nd Sensor	3rd Sensor	1st Sensor	2nd Sensor	3rd Sensor	
40 dB	Exhaustive Annealing	3	380	465	615	250	80	210	2.4 $\pm$ 1.1
			<b>380</b>	<b>460</b>	<b>630</b>	<b>180</b>	<b>80</b>	<b>120</b>	2.4 $\pm$ 1.1
	Exhaustive Annealing	4	<b>380</b>	<b>465</b>	<b>635</b>	<b>280</b>	<b>70</b>	<b>190</b>	<b>2.4 <math>\pm</math> 1.2</b>
			<b>380</b>	<b>465</b>	<b>635</b>	<b>280</b>	<b>70</b>	<b>190</b>	<b>2.4 <math>\pm</math> 1.2</b>
	Exhaustive Annealing	5	<b>395</b>	<b>475</b>	<b>630</b>	<b>260</b>	<b>60</b>	<b>250</b>	<b>2.5 <math>\pm</math> 1.2</b>
			<b>395</b>	<b>475</b>	<b>630</b>	<b>260</b>	<b>60</b>	<b>250</b>	<b>2.5 <math>\pm</math> 1.2</b>
30 dB	Exhaustive Annealing	3	<b>380</b>	<b>465</b>	<b>595</b>	<b>170</b>	<b>90</b>	<b>120</b>	<b>4.8 <math>\pm</math> 2.2</b>
			<b>380</b>	<b>465</b>	<b>595</b>	<b>170</b>	<b>90</b>	<b>120</b>	<b>4.8 <math>\pm</math> 2.2</b>
	Exhaustive Annealing	4	395	470	620	250	80	190	5.0 $\pm$ 2.3
			395	470	620	230	70	180	5.0 $\pm$ 2.3
	Exhaustive Annealing	5	<b>395</b>	<b>465</b>	<b>615</b>	<b>250</b>	<b>80</b>	<b>190</b>	<b>4.9 <math>\pm</math> 2.1</b>
			<b>395</b>	<b>465</b>	<b>615</b>	<b>250</b>	<b>80</b>	<b>190</b>	<b>4.9 <math>\pm</math> 2.1</b>
26 dB	Exhaustive Annealing	3	<b>395</b>	<b>460</b>	<b>550</b>	<b>100</b>	<b>60</b>	<b>90</b>	<b>7.3 <math>\pm</math> 4.1</b>
			<b>395</b>	<b>460</b>	<b>550</b>	<b>100</b>	<b>60</b>	<b>90</b>	<b>7.3 <math>\pm</math> 4.1</b>
	Exhaustive Annealing	4	<b>385</b>	<b>460</b>	<b>605</b>	<b>200</b>	<b>70</b>	<b>150</b>	<b>7.1 <math>\pm</math> 3.2</b>
			<b>385</b>	<b>460</b>	<b>605</b>	<b>200</b>	<b>70</b>	<b>150</b>	<b>7.1 <math>\pm</math> 3.2</b>
	Exhaustive Annealing	5	395	470	605	220	70	160	6.7 $\pm$ 3.0
			400	465	605	200	70	160	6.9 $\pm$ 2.8

<sup>a</sup>Cases where the annealing and exhaustive searches found the same solution are in bold type.

Something similar occurs when we quantize at either 12, 10, or 8 bits, as seen in Fig. 3 for the case of 5 sensors, 5 eigenvectors, and an SNR of 30 dB. Results improve if we use 12 bits rather than 8 bits, but the difference is small. Thus we can use a cheaper and faster 8-bit A/D converter without significantly degrading system accuracy. In fact, the most important step in building a multispectral imaging system is to optimize the sensors for the remote-sensing task at hand rather than to increase their number or quantization levels, both of which will increase system cost and response time.

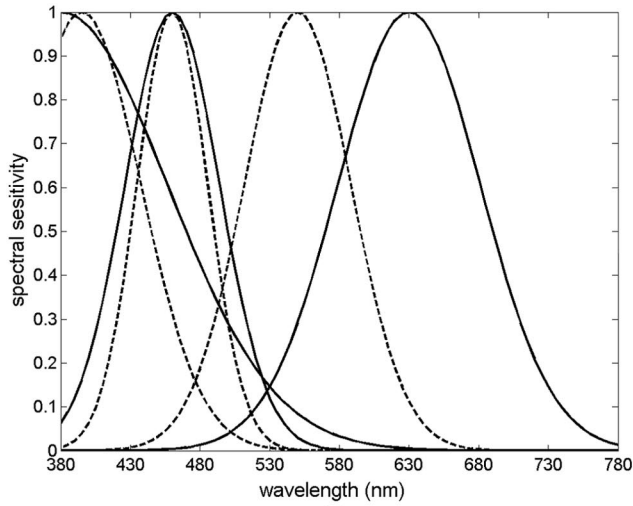
For high-noise (low SNR) sensors, increasing the number of eigenvectors from 3 to 5 is always pref-

erable, whereas adding more sensors simply increases system noise. This can be appreciated by noting that a system with more sensors likely has more connections, more transistors in the CCD, and more memory cells. All these elements individually contribute noise, and so each raises the total noise level. As other authors have noted,<sup>1,7,10</sup> spectral recoveries do not improve significantly in noise-free simulations if the number of sensors increases from, say, four to seven (the particular numbers of sensors depend on system hardware and on the shapes of the skylight spectra). If we add noise to such simulations, using more sensors increases the noise in matrix  $\Lambda$ . This noise propagates through-

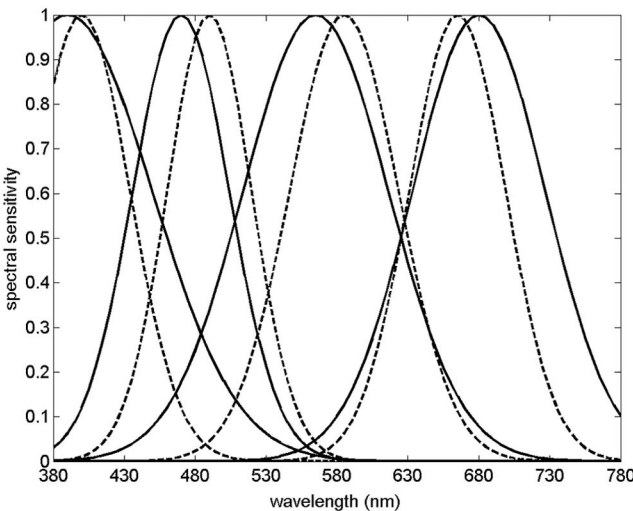
**Table 3. Comparison of Best 3 Sensors Found Using Annealing Searches with Various Metrics, 3 Eigenvectors, and the Granada Skylight Spectra<sup>a</sup>**

Cost Function	Peak Sensitivities (nm)			FWHM (nm)			GFC $\pm$ SD	$\Delta E^*_{ab}$ $\pm$ SD	IIE(%) $\pm$ SD	CSCM $\pm$ SD
	1st Sensor	2nd Sensor	3rd Sensor	1st Sensor	2nd Sensor	3rd Sensor				
GFC	400	470	645	50	40	60	<b>0.9994 <math>\pm</math> 0.0012</b>	0.8 $\pm$ 0.6	1.3 $\pm$ 0.7	2.5 $\pm$ 1.1
$\Delta E^*_{ab}$	445	525	605	30	40	50	0.9923 $\pm$ 0.0131	<b>0.3 <math>\pm</math> 0.2</b>	2.3 $\pm$ 1.6	4.3 $\pm$ 2.3
IIE(%)	470	475	720	20	250	290	0.9972 $\pm$ 0.0040	1.3 $\pm$ 0.8	<b>0.7 <math>\pm</math> 0.5</b>	3.2 $\pm$ 1.4
CSCM	380	460	630	180	80	120	0.9993 $\pm$ 0.0012	0.7 $\pm$ 0.5	1.3 $\pm$ 0.7	<b>2.4 <math>\pm</math> 1.1</b>

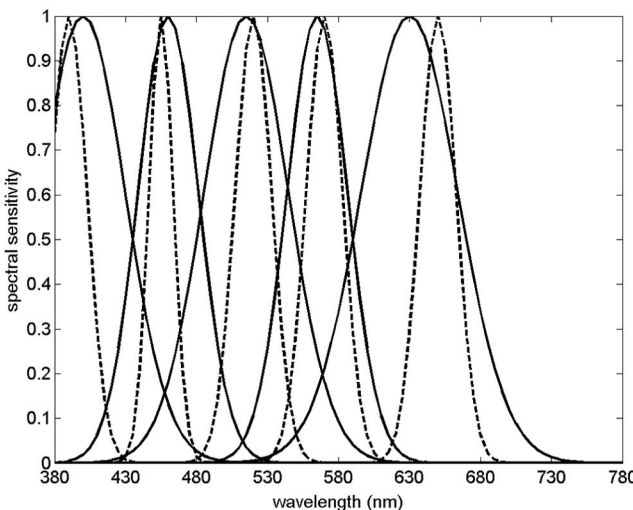
<sup>a</sup>SNR = 40 dB, and quantization is at 12 bits. The best result for each metric appears in bold type, when it alone was the annealing algorithm's cost function.



(a)



(b)



(c)

Fig. 1. Each row shows the spectral sensitivity curves of the best 3-, 4-, or 5-sensor systems, respectively (the numbers of eigenvectors and sensors are equal in each case). Solid curves represent sensors for SNR = 40 dB, while dashed curves represent sensors for SNR = 26 dB.

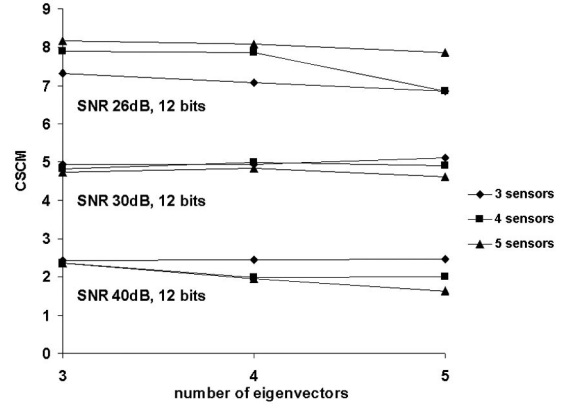


Fig. 2. Means for the CSCM metric for 1567 skylight spectra measured in Granada, Spain, using 3–5 sensors and 3–5 eigenvectors at 12-bit quantization for various SNR.

out the mathematical path described in Section 2 and degrades system performance more than the additional sensors improve it.<sup>7,10</sup>

Several steps are needed to implement a working multispectral system such as those simulated here. First, we must establish *a priori* the accuracy required of the system. Second, we must reduce noise by all practical means (e.g., cooling the CCD and subtracting its dark noise). Finally, we must decide how many sensors our system will have, select a preferred A/D converter, and calculate both the system's desired response times and cost.

Naturally our system must work for spectra other than those used to calculate the original dataset's eigenvector matrix  $V$ . Thus we extend our analysis to skylight spectra measured at another site in Owings, Maryland. Using 12-bit quantization and the best set of sensors found for each case (see Table 4), we analyze metrics for these new spectra in bold-type rows in Table 4. It too shows small errors for the recovered spectra, demonstrating that both our spectral recovery method and optimum sensors can be used to develop a reliable system for imaging skylight spectra. Note that although mean GFC and CIELAB  $\Delta E^*_{ab}$  are similar for the Owings spectra, mean IIE(%) is

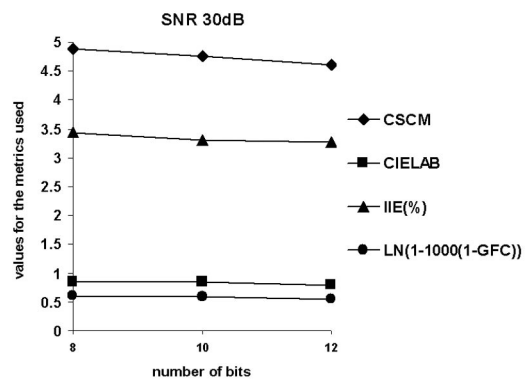


Fig. 3. Effects of quantization noise: mean values for metrics of the Granada skylight spectra using 5 sensors and 5 eigenvectors for SNR = 30 dB.

Table 4. Means for the Granada Skylight Spectral Recoveries Using the Best Sets of 3 to 5 Sensors for Various SNR Levels and 12-Bit Quantization<sup>a</sup>

SNR	Number of Sensors	Number of Eigenvectors	GFC $\pm$ SD	$\Delta E^*_{ab} \pm$ SD	IIE(%) $\pm$ SD	CSCM $\pm$ SD
40 dB	3	3	0.9993 $\pm$ 0.0012	0.7 $\pm$ 0.5	1.3 $\pm$ 0.7	2.4 $\pm$ 1.1
	3	5	0.9988 $\pm$ 0.0023	1.0 $\pm$ 0.6	0.9 $\pm$ 0.6	2.5 $\pm$ 1.2
	4	3	0.9994 $\pm$ 0.0011	0.8 $\pm$ 0.6	1.2 $\pm$ 0.7	2.4 $\pm$ 1.2
	4	4	0.9997 $\pm$ 0.0003	0.6 $\pm$ 0.3	1.2 $\pm$ 0.5	2.0 $\pm$ 0.7
	5	3	0.9993 $\pm$ 0.0012	0.8 $\pm$ 0.5	1.1 $\pm$ 0.7	2.3 $\pm$ 1.2
	5	5	0.9998 $\pm$ 0.0002	0.3 $\pm$ 0.2	1.1 $\pm$ 0.8	1.6 $\pm$ 0.8
	<b>5</b>	<b>5</b>	<b>0.9990 <math>\pm</math> 0.0002</b>	<b>0.2 <math>\pm</math> 0.1</b>	<b>0.5 <math>\pm</math> 0.4</b>	<b>1.5 <math>\pm</math> 0.5</b>
30 dB	3	3	0.9987 $\pm$ 0.0016	0.9 $\pm$ 0.5	3.2 $\pm$ 1.9	4.8 $\pm$ 2.2
	3	5	0.9939 $\pm$ 0.0067	1.6 $\pm$ 0.7	1.7 $\pm$ 1.4	4.9 $\pm$ 2.1
	4	3	0.9990 $\pm$ 0.0017	0.9 $\pm$ 0.4	3.5 $\pm$ 2.1	4.9 $\pm$ 2.4
	4	4	0.9991 $\pm$ 0.0008	0.9 $\pm$ 0.5	3.5 $\pm$ 1.4	4.9 $\pm$ 1.8
	5	3	0.9985 $\pm$ 0.0017	1.1 $\pm$ 0.6	2.8 $\pm$ 1.6	4.7 $\pm$ 2.0
	5	5	0.9991 $\pm$ 0.0009	0.8 $\pm$ 0.4	3.3 $\pm$ 2.1	4.6 $\pm$ 2.3
	<b>5</b>	<b>5</b>	<b>0.9984 <math>\pm</math> 0.0009</b>	<b>0.7 <math>\pm</math> 0.3</b>	<b>1.7 <math>\pm</math> 1.3</b>	<b>3.3 <math>\pm</math> 1.6</b>
26 dB	3	3	0.9981 $\pm$ 0.0023	1.3 $\pm$ 0.7	5.0 $\pm$ 3.5	7.3 $\pm$ 4.1
	3	5	0.9867 $\pm$ 0.0132	2.0 $\pm$ 0.7	2.4 $\pm$ 2.1	6.9 $\pm$ 2.8
	4	3	0.9986 $\pm$ 0.0017	1.2 $\pm$ 0.6	5.9 $\pm$ 2.9	7.9 $\pm$ 3.2
	4	5	0.9902 $\pm$ 0.0014	2.0 $\pm$ 0.8	2.7 $\pm$ 2.2	6.9 $\pm$ 3.1
	5	3	0.9976 $\pm$ 0.0025	1.4 $\pm$ 0.7	5.7 $\pm$ 3.1	8.2 $\pm$ 3.5
	5	5	0.9988 $\pm$ 0.0012	1.1 $\pm$ 0.5	6.1 $\pm$ 2.6	7.9 $\pm$ 3.1
	<b>3</b>	<b>5</b>	<b>0.9970 <math>\pm</math> 0.0018</b>	<b>1.6 <math>\pm</math> 0.7</b>	<b>1.9 <math>\pm</math> 1.4</b>	<b>4.9 <math>\pm</math> 2.6</b>

<sup>a</sup>Rows in bold type are the means for 242 skylight spectra measured in Owings recovered with the best set of sensors at 12-bit quantization.

always less for the smaller Owings dataset than for the larger one from Granada. This occurs because the Owings spectra are from a limited range of solar elevations and are spectrally similar to most of the Granada data. Both factors make the Granada eigenvectors well matched to those that we could calculate independently for Owings. The few spectra measured at low solar elevations in Granada exert relatively little influence on the PCA eigenvectors, and these Granada spectra are the ones that increase the mean Granada IIE(%). Yet even the least accurate recoveries of skylight spectra at Owings (see Fig. 4) show relatively small differences between the original and recovered spectra.

### 6. Conclusions

We have shown that linear methods based on PCA allow accurate recovery of skylight spectra from broadband camera sensors. We propose CSCM as a single metric that takes into account three different accuracy standards: spectral, colorimetric, and total integrated irradiance. Our CSCM metric can easily be used instead of CIELAB or RMSE alone in search algorithms. We have presented a simulated annealing algorithm, using CSCM as a single cost function, as a fast method for searching a limited number of Gaussian sensors to construct an optimum multispectral imaging system. We have simulated some common noise sources present in any digital imaging system in order to mimic noise in real images. We have shown that increasing the number of sensors does not necessarily improve the accuracy of recov-

ered spectra if sensor noise is high because each sensor's individual noise contributions degrade the overall quality of the spectral reconstruction. Thus the optimum number of sensors depends on noise levels inherent to the given multispectral system.

Skylight has complicated spectra with different absorption bands that depend on species such as water vapor, molecular oxygen, ozone, and aerosols, and the relative strength of these bands varies daily and even hourly. Yet despite this ever-changing spectral detail, we find that a linear recovery algorithm using only a

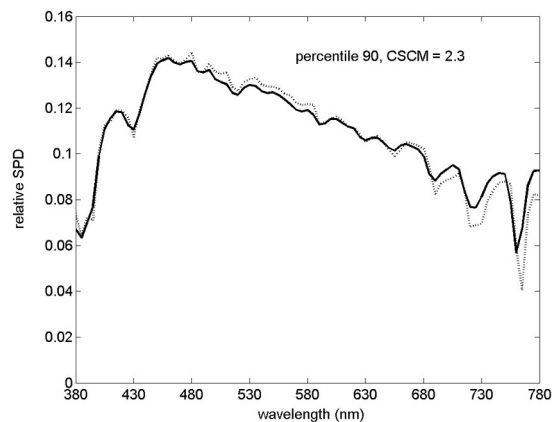


Fig. 4. Original skylight spectrum (solid curve) measured in Owings, Maryland, and recovered (dotted curve) spectrum for SNR = 40 dB with 5 sensors, 5 eigenvectors, and 12-bit quantization for the 90th percentile of the CSCM.

few optimum Gaussian sensors returns high-quality reconstructions of skylight spectra, even with sensor noise. In future work, we will use a LCTF and a monochrome camera to build the sensors simulated here in order to study their actual performance in recovering skylight spectra.

M. López-Álvarez thanks Consejería de Innovación y Desarrollo Tecnológico de la Junta de Andalucía for the grant that supports his investigation. J. Hernández-Andrés and J. Romero were supported by Spain's Comisión Interministerial de Ciencia y Tecnología (CICYT) under research grant DPI 2004-03734. R. L. Lee was supported by United States National Science Foundation grant ATM-0207516 and by the United States Naval Academy's Departments of Physics and Mathematics.

## References

1. J. Hernández-Andrés, J. L. Nieves, E. M. Valero, and J. Romero, "Spectral-daylight recovery by use of only a few sensors," *J. Opt. Soc. Am. A* **21**, 13–23 (2004).
2. J. Hernández-Andrés, J. Romero, and R. L. Lee, Jr., "Colorimetric and spectroradiometric characteristics of narrow-field-of-view clear skylight in Granada, Spain," *J. Opt. Soc. Am. A* **18**, 412–420 (2001).
3. J. Hernández-Andrés, J. Romero, and R. L. Lee, Jr., "Calculating correlated color temperatures across the entire gamut of daylight and skylight chromaticities," *Appl. Opt.* **38**, 5703–5709 (1999).
4. J. Hernández-Andrés, R. L. Lee, Jr., and J. Romero, "Color and luminance asymmetries in the clear sky," *Appl. Opt.* **42**, 458–464 (2003).
5. J. Y. Hardeberg (2001), "Acquisition and reproduction of color images: colorimetric and multispectral approaches" (Dissertation.com, Parkland, Fla., 2001) (revised second edition of Ph.D. dissertation, Ecole Nationale Supérieure des Télécommunications, Paris, 1999), pp. 157–174.
6. D. Connah, S. Westland, and M. G. A. Thomson, "Optimization of a multispectral imaging system," in *Proceedings of the 1st European Conference on Colour Graphics, Image and Vision* (Society for Imaging Science and Technology, Springfield, Va., 2002), pp. 619–622.
7. N. Shimano, "Optimal spectral sensitivities of a color image acquisition device in the presence of noise," in *Proceedings of the 2nd European Conference on Colour Graphics, Imaging and Vision* (Society for Imaging Science and Technology, Springfield, Va., 2004), pp. 379–383.
8. L. T. Maloney and B. A. Wandell, "Color constancy: a method for recovering surface spectral reflectance," *J. Opt. Soc. Am. A* **3**, 29–33 (1986).
9. D. H. Marimont and B. A. Wandell, "Linear models of surface and illuminant spectra," *J. Opt. Soc. Am. A* **9**, 1905–1913 (1992).
10. D. Connah, S. Westland, and M. G. A. Thomson, "Recovering spectral information using digital camera systems," *Color Technol.* **117**, 309–312 (2001).
11. J. Romero, A. García-Beltrán, and J. Hernández-Andrés, "Linear bases for representation of natural and artificial illuminants," *J. Opt. Soc. Am. A* **14**, 1007–1014 (1997).
12. P. D. Burns, "Analysis of image noise in multispectral color acquisition," Ph.D. dissertation (Rochester Institute of Technology, 1997).
13. P. D. Burns and R. S. Berns, "Quantization in multispectral color image acquisition," in *Proceedings of the 7th Color Imaging Conference: Color Science, Systems and Applications* (IS&T, Scottsdale, Arizona, 1999), pp. 32–35.
14. D. C. Day, "Filter selection for spectral estimation using a trichromatic camera," Ph.D. dissertation (Rochester Institute of Technology, 2003).
15. F. H. Imai, R. S. Berns, and D. Y. Tzeng, "A comparative analysis of spectral reflectance estimated in various spaces using a trichromatic camera system," *J. Imag. Sci. and Technol.* **44**, 280–287 (2000).
16. G. Buchsbaum and O. Bloch, "Color categories revealed by non-negative matrix factorization of Munsell color spectra," *Vis. Res.* **42**, 559–563 (2002).
17. Y. Yokoyama, N. Tsumura, H. Haneishi, J. Hayashi, and M. Saito, "A new color management system based on human perception and its application to recording and reproduction of art paintings," in *Proceedings of the 5th Color Imaging Conference: Color Science, Systems and Applications* (Society for Imaging Science and Technology, Springfield, Va., 1997), pp. 169–172.
18. S. Franco, *Design with Operational Amplifiers and Analog Integrated Circuits*, 3rd ed. (McGraw-Hill, Boston, 2002), pp. 311–346.
19. J. Y. Hardeberg, "Filter selection for multispectral color image acquisition," in *Proceedings of PICS 2003* (Society for Imaging Science and Technology, Springfield, Va., 2003), pp. 177–182.
20. F. H. Imai, M. R. Rosen, and R. S. Berns, "Comparative study of metrics for spectral match quality," in *Proceedings of the 1st European Conference on Colour in Graphics, Image and Vision*, pp. 492–496 (2002).
21. R. G. Kuehni, *Color Space and its Divisions: Color Order from Antiquity to the Present*, 1st ed. (Wiley, New York, 2003), pp. 204–270.
22. M. R. Luo, G. Cui, and B. Rigg, "The development of the CIE 2000 colour-difference formula: CIEDE2000," *Color Res. Appl.* **26**, 340–350 (2001).
23. G. Wyszecki and W. S. Stiles, *Color Science: Concepts and Methods, Quantitative Data and Formulae*, 2nd ed. (Wiley, New York, 1982), pp. 117–248.
24. J. A. S. Viggiano, "Metrics for evaluating spectral matches: a quantitative comparison," in *Proceedings of the 2nd European Conference on Colour Graphics, Imaging and Vision* (Society for Imaging Science and Technology, Springfield, Va., 2004), pp. 286–291.
25. J. A. S. Viggiano, "A perception-referenced method for comparison of radiance ratio spectra and its application as an index of metamerism," *Proc. SPIE* **4421**, 701–704 (2002).
26. J. J. Michalsky, "Estimation of continuous solar spectral distributions from discrete filter measurements: II. A demonstration of practicability," *Sol. Energy* **34**, 439–445 (1985).
27. W. H. Press, S. A. Teukolsky, W. T. Vetterling, and B. P. Flannery, *Numerical Recipes in C: The Art of Scientific Computing* (Cambridge University, 1992).
28. N. Metropolis, A. Rosenbluth, M. Rosenbluth, A. Teller, and E. Teller, "Equations of state calculations by fast computing machines," *J. Chem. Phys.* **21**, 1087–1092 (1953).